Mediterranean Archaeology and Archaeometry, Vol. 16, No 1,(2016), pp. 193-202

DOI: 10.5281/zenodo.35532

PHYSICAL, MECHANICAL AND MICROSTRUCTURAL CHARACTERIZATION OF BASILICA PLASTERS AND BOULEUTERION MORTARS IN SMYRNA AGORA

Burak Felekoğlu[1], Eren Gödek*[2] Akın Ersoy[3], İ.Murat Kuşoğlu[4], Altuğ Hasözbek[4]

[1]Dokuz Eylül University, Engineering Faculty, Department of Civil Enginneering, Buca, İzmir, Turkey
[2] The Graduate School of Natural and Applied Science, Constr. Materials Program, Buca, İzmir, Turkey
[3] Dokuz Eylül University, Faculty of Letter, Department of Archeology, Buca, İzmir, Turkey
[4] Dokuz Eylül University, Archaeometry Application & Research Center, Torbalı, İzmir, Turkey

Received: 11/09/2015
Accepted:10/12/2015
Corresponding author: Eren Gödek (eren.godek@ogr.deu.edu.tr)

ABSTRACT

Lime based plaster and mortar specimens from three different locations of Smyrna Agora excavations have been investigated within the scope of this study. A two-layer graffito plaster from Basilica (P1 inner layer, P2 outer layer) and two distinctive mortars from Bouleuterion were collected from the site. While one of the Bouleuterion mortars was masonry mortar from walls (BWM), other one was from the floor blockade (BBM – porous mortar).

Physical and mechanical properties of plaster and mortar specimens such as water absorption, density and surface hardness and compressive strength have been determined. Thin section analyses were performed for mineralogical investigations. Aggregate particle size distribution of both plaster and mortar specimens were determined by sieve analysis. The fraction passing through 0.063 mm sieve was considered as the binder. Powder fractions of 0-0.063 mm and 0.063-0.125 mm were used in X-ray Diffraction (XRD) analysis for the comparison and characterization of binder and aggregate crystal structure respectively. The chemical composition of polished sections of plaster and mortar specimens were also investigated by Scanning Electron Microscope equipped with an Energy Dispersive Spectrometer (SEM-EDS).

Test results showed that outer plaster layer (P2) is denser, harder and exhibited higher strength compared to inner plaster layer P1. This strength difference can be attributed to the possibly low water/lime ratio of P2 plaster in order to finish the outer surface of plaster by pressurized troweling. By this way, it is possible to obtain a smooth surface suitable for graffito applications.

High compressive strength and surface hardness of Bouleuterion wall mortars (BWM) is due to the presence of crushed brick particles as aggregates which provides a good aggregate-matrix bonding. This improved bonding can be attributed to the pozzolanic activity of crushed brick particles with lime mortar. Dense matrix structure is also responsible for the relatively high mechanical performance of BWM. On the other hand, porous structure of floor blockade mortar located between stones results with low strength and hardness.

KEYWORDS: plaster, mortar, surface hardness, water absorption, XRD, SEM-EDS, compressive strength.

1. INTRODUCTION

"New/Nea" Smyrna has been founded on the slopes of Kadifekale towards Kemeraltı after Alexander the Great. The city was founded at the end of 4. Century B.C.-beginning of 3. Century B.C. by Antigonos Monophtalmos and Lysimakhos according to ancient sources and the most known and researched site in the city is the Agora. Agora of Smyrna occupies a rectangular area in the center of the city and its courtyard is surrounded on four sides with Hellenistic Stoas. After Smyrna is under Roman rule it is understood that these stoas were not enough to satisfy the needs of the new rule and had to be rearranged.

Northern stoa has been transformed into a basilica with 4 galleries on the basement and 3 galleries on the ground level. While the 3 galleries of the basement of the basilica which is well preserved are ordinary galleries the 4th gallery has a different plan. Most important feature of the Basilica is one of the biggest grafiti collections of ancient world giving us extensive information about the ancient world preserved on 2 separate layers of plaster on the walls of the 1st and 2nd galleries of the basement. It is thought that there are three thousand grafiti on the walls ranging from a single letter to depictions in paint (dipinti) or incised. Graffiti in the Basilica is thought to be made between 2nd and 4th century and the plaster with the grafiti on is important to understand the technology to produce this plaster with regards to differences and similarities to the contemporary examples in other ancient cities.

The Bouleuterion which is located beyond the Western Stoa/Portico of the courtyard shows Roman structural features and is thought to be built at the end of the 2nd century. Bouleuterion stands on a foundation of rubble mixed with spolia filling with lime mortar on a filled terrace. The building is in a small theatre form and its vaulted substructure rising on bearing walls carries marble seating. Analysis of the plaster and filling of the Bouleuterion bearing walls carrying immense weights is important in order to understand the technique and the building material of the building itself and to see the similarities with contemporary examples.

Lime based plaster and mortar specimens from three different locations of Smyrna Agora excavations have been investigated within the scope of this study. A two-layer graffito plaster from Basilica (P1 inner layer, P2 outer layer) and two distinctive mortars from Bouleuterion were collected from the site. While one of the Bouleuterion mortars was masonry mortar from walls (BWM), other one was from the floor blockade (BBM – porous mortar). Physical and mechanical properties of plaster and mortar specimens such as water absorption, density and surface hardness and compressive strength have been determined. Furthermore optical and scanning microscope based petrography and XRD based analysis have been performed on binder and aggregate phases of plaster and mortar specimens.

2. PLASTER AND MORTAR CHARACTERIZATION STUDIES

2.1 Sampling locations and labels

Location of plaster and mortar specimens at the excavation site are marked in Figure 1. Two layer graffito plaster particles (approximately 100-150 g) detached from Basilica walls can be seen in Figure 2. Outer (P2) and inner (P1) layers were easily separated at some locations of Basilica walls. Both layers were individually investigated and visual investigations revealed that outer layer was more dense, thinner and hard compared to inner layer.

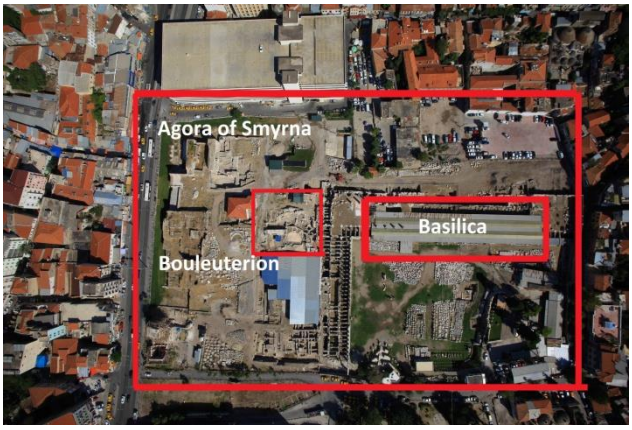

Figure 1. Locations of sampling points at the excavation site.

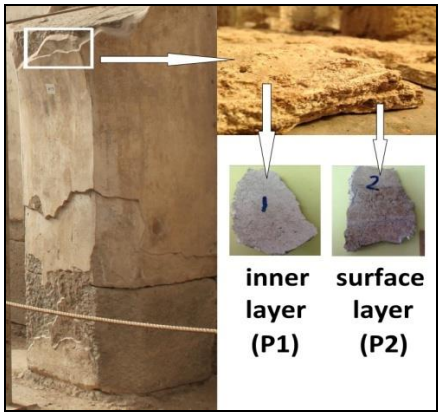

Figure 2. Two-layer graffito plaster detached from Basilica walls (P1-P2)

Blockade mortar between stones was detached from Bouleuterion (BBM). It was a weak and porous mortar used for filling the spaces between blockade stones. Approximately 50-100 g of mortar was collected from the site shown in Figure 3. Another mor-

tar samples were collected from a newly exposed fractured surface of mortar from Bouleuterion walls (BWM). It was a hard, dense and sound mortar with visible brick fragments at fracture surface (Figure 4).

Figure 3. Bouleuterion blockade mortar between stones (BBM).

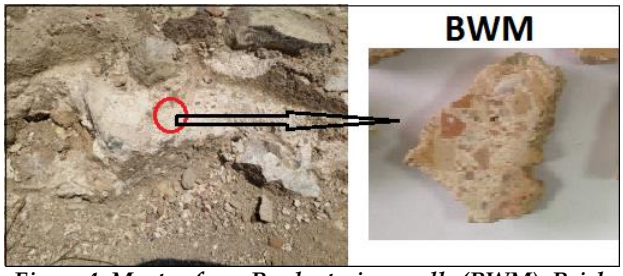

Figure 4. Mortar from Bouleuterion walls (BWM). Brick fragments can be seen at the newly exposed fractured surface of mortar.

2.2 Water absorption and bulk density measurements

Water absorption percentage is determined by dividing the weight change of each specimen submerged in water. Minimum 5 pieces (within the range of 1-6 g) were tested for each mortar. Before immersion in water, specimens dried in an oven at 105°C for one day. Initial weight is measured with milligram precision weigher (Figure 5a). Specimens kept in water for one week and then final weight is measured. Excess surface water is removed with a napkin before final weight measurement. Bulk density of plaster and mortar specimens were determined by dividing the dry weight of each specimen particle to its volume. The volumes of particles were measured with a hand-made mini-Archimedes balance suitable by determining the weight of small specimens under water (Figure 5b, c). Before weight measurement specimen particles were fully saturated with water. Water absorption and bulk density test results are listed in Table 1.

(a) *(b)* *(c)*

Figure 5. a) Milligram precision weigher for measuring dry weight, b) Sample chamber assembly, c) Weight measurement of specimen particle under water.

2.3 Surface hardness and compressive strength measurements

A pendulum type Schmidt hammer (Proceq) was used in order to determine the surface hardness of plaster and mortars (de Vekey., 1997). The pendulum of Schmidt hammer is allowed to free fall and hit the specimen surface. The rebound height of the pendulum is recorded as rebound number (or hardness number) (Figure 6). This hammer is suitable to measure surface hardness of lightweight concrete and low strength mortars at a compressive strength interval of 1-10 MPa. Schmidt hammer hardness number is insignificant for very low strength mortars (compressive strength less than 1 MPa). It should be noted that surface hardness of cement and lime based mortars can not always be correlated with compressive strength due to existence of time dependent carbonation reactions and porosity differences (Schueremans et al., 2011). For this reason, Schmidt hammer rebound number can be used as a quality control value for mortars with equivalent ages.

At least four specimens tested with pendulum type Schmidt hammer. Due to the geometrical compatibility plaster sample specimens (constant thickness), they were vertically fixed to a flat surface with a band. Schmidt hammer is located to hit the specimen surface and rebound number is measured. As seen in Figure 6, there was no problem and rebound number is determined for P2 specimens. However, no rebound value was recorded due to the low strength of P1 specimens. P1 specimens damaged with the hammer hit (Figure 7). Mortar specimens were geometrically irregular and they should be cut in parallel before hammer testing. BWM specimen particles were easily cut and tested due to their sufficiently high strength. However, BBM specimens fractionated while cutting and no Schmidt rebound number was obtained from the fractured pieces. It is possible to evaluate that the strength grade of P1 and BBM are less than 1 MPa which is out of the measur-

ing range of pendulum type Schmidt hammer. Test results are presented in Table 1.

Plaster and mortars are classified by Proceq Schmidt OS-120 (2014) pendulum hammer catalogue as a function of hammer rebound number. According to this classification, rebound numbers between 0-20, 20-30, 30-40, 40-55, 55-75, 75-100 are called as weak, average, acceptable, good, very good and perfect quality, respectively. P2 plaster and BWM mortar with average rebound numbers of 28 and 37 can be classified as average and acceptable quality mortars.

Figure 6. Surface hardness measurement of P2 specimen with Pendulum type Schmidt hammer (Sound specimens with no damage after pendulum hammer hit)

Figure 7. Surface hardness measurement of P1 specimen with Pendulum type Schmidt hammer (Crushing and fracture **of specimen after pendulum hammer hit)**

Compressive strength of plaster and mortar specimens were determined with a new developed methodology. According to TS EN 196 standard, mortar specimen size for flexural and compressive testing is 40*40*160 mm^3. However, the thickness of plaster specimens are extremely small (10 mm), and thus it is not possible to obtain standard size specimens from these samples. A wooden loading frame is built in order to load the specimens at a 10*10 mm^2 cross sectional area (Figure 8). Since the thickness is approximately 10 mm, the loaded specimen dimension can be accepted as a cube with 10*10*10 mm^3. Plaster layer is ground or cut down to the same height if plaster layer was thicker. Compressive strength values are listed in Table 1. Since lime based mortars are porous materials, their compressive strength is size sensitive. The so called "size effect" should be taken into consideration in order to compare the compressive strength values with standard specimen dimensions. Alejandre et al. (2014), experimentally showed that micro-specimens overestimate the compressive strength of mortars prepared with standard size specimens and proposed conversion coefficients were at the range of 0.65 to 0.86. These coefficients can be used to normalize the compressive strength of micro-specimens (as small as 15*15*15 mm^3) to standard size (40*40*40 mm^3) specimens. Having these coefficients allows us to transform the compressive strength of specimens from mortars collected on site into strength values determined for standard/normalized specimens in order to gain a better characterization to aid in mortar substitutions or restoration (Alejandre et al., 2014). Conversion coefficient of 0.50 was determined by extrapolating the coefficient value to 10*10*10 mm^3 specimen size. Due to this reason, the compressive strength values of 10*10*10 mm^3 mortar specimens were divided by 2 to convert into standards size specimen (40*40*40 mm^3) values. As seen in Table 1, normalized compressive strength of P1 plaster and BBM mortar were extremely low and it is possible to break them into pieces by hand. On the other hand, normalized compressive strength of 3.28 MPa and 4.54 MPa values were derived from P2 and BWM specimens. Normalized compressive strength values of P2 and BWM are as high as today's NHL2 or HL2 class lime mortars. According to EN 459 standard classifications, 28 days compressive strength of Natural Hydraulic Lime (NHL2) or Hydraulic Lime (HL2) is between 2-7 MPa.

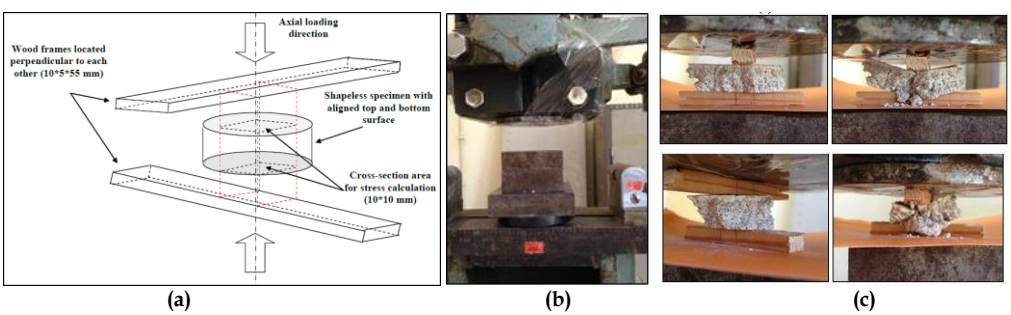

Figure 8. a) Loading frame scheme designed for axial compressive strength test of plaster and mortar specimens, b) Loading setup photograph, c) Specimens before loading (on the left) and after compression failure (on the right).

Table 1. Physical and mechanical properties of plaster and mortars

Sample label	Water absorption (%)	Bulk density (g/cm³)	Surface hardness (rebound number)	10*10 mm² Compressive strength[1] (MPa)	Normalized[2] Compressive strength (MPa)
P1[3]	25.6±3.4	1.38±0.10	0	0.14±0.07	0.07
P2[4]	19.2±0.7	1.64±0.08	28±4	6.56±0.81	3.28
BBM[5]	27.3±4.7	1.29±0.22	0	0.31±0.06	0.16
BWM[6]	9.2±1.1	1.82±0.18	37±9	9.07±1.02	4.54

1. *Compressive strength of specimens loaded at a cross-section of 10*10 mm².*
2. *Corrected (normalized) compressive strength for an imaginary loading cross-section of 40*40 mm² due to size effect.*
3. *Inner plaster layer from Basilica*
4. *Outer plaster layer from Basilica*
5. *Bouleuterion floor blockade mortar*
6. *Bouleuterion wall mortar*

2.4 Sieve analysis of plaster and mortar aggregates

Identification of plaster and mortar types requires the granulometric analysis of samples by mechanical sieving. For this purpose plaster and mortar specimens gently ground in an agate mortar. Care was taken not to crush aggregates. This method has proved its success, if plaster or mortar is weak in terms of aggregate matrix bonding ability (Figure 9). However, if aggregate-matrix bond is strong, the grounding affect may also cause the fracture of some aggregates. In this case, underestimation of aggregate particle size distribution from the actual value can be expected (Figure 10). ISO 565 series sieve meshes of 8, 4, 2, 1, 0.500, 0.250, 0.125 and 0.063 mm were used and the granulometry curves are plotted in Figure 11 (Moropoulou et al., 2000). Granulometry of pure aggregate phase can also be obtained by sieving mortar remnants after dissolution in dilute HCl. However, in that case the carbonates based aggregate will be lost during the acid attack (Franzini et al., 2000). Due to this reason, only mechanical separation technique (by gently grounding in agate mortar) is used.

Figure 9. Aggregates of P1 plaster sieved by ISO 565 series meshes (4, 2, 1, 0.500, 0.250, 0.125 and 0.063 mm). All aggregates of P1 passed 4 mm meshes.

(a) ***(b)***

Figure 10. Aggregates of a) BBM and b) BWM mortars sieved by ISO 565 series meshes (8, 4, 2, 1, 0.500, 0.250, 0.125 and 0.063 mm). All aggregates of BBM and BWM passed 8 mm meshes.

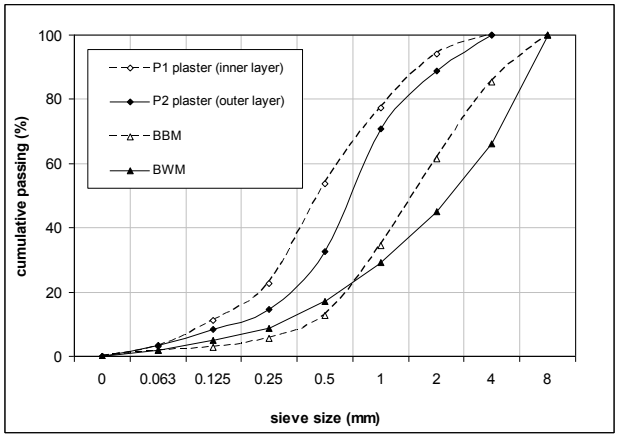

Figure 11. Particle size distribution curves of P1, P2 plasters, BBM and BWM mortar aggregates

2.5 Thin section analysis of plaster and mortars

Thin section analyses were performed on the samples of P1, P2, BWM, and BBM respectively. Thin sections were prepared from the sample chips and thinned out to 30 μm for interpreting the petrographic features such as texture, mineral-rock fragment abundance with classification and sample dependent micro-features. A polarizing microscope (Olympus BX41 Trinocular Pol) equipped with a digital Olympus 7.1 Mp C-7070 digital camera was used and micro-photos were captured at Cross-Polarized Light (XPL) and Parallel Polarized Light (PPL)

modes. Petrographical analyses are made in order to determine the mineral type and structure of the mortar's aggregate and binder phases.

2.6 SEM-EDS analysis of plasters and mortars

The semi-quantitative chemical composition of polished sections of plaster and mortar specimens were investigated by a Jeol JSM 6060 Scanning Electron Microscope equipped with an Energy Dispersive Spectrometer (SEM-EDS). SE images captured at 10 kV were employed for this purpose. In addition to regional elemental analysis of each mortar specimen, line analysis is performed in plaster layers in order to investigate the elemental composition variation specimen depth. Main elements searched in analyzed were Ca, Si, Al, Fe, K, Na, Mg respectively.

2.7 XRD analysis of powdered plaster and mortars

The granulometric fractions of < 63 μm and 0.063-0.125 mm of plaster and mortar specimens obtained from sieve analysis were used in XRD analysis. The fraction of < 63 μm was assumed as the binder phase. A little amount of fine grain aggregate frequently present in the fractions of 0.063-0.125 mm. Approximately 1.5-2 g of the fine powder was used for XRD analysis. Rigaku D/Max-200/PC model x-ray diffractometer with a Cu-target x-ray tube is used at 40 kV voltage and 36 mA current. Data is collected between 2θ= 3-60º with a scanning rate of 2º/min.

3. RESULTS AND DISCUSSION

3.1 Physical and mechanical properties

The water absorption, bulk density, surface hardness and normalized compressive strength test results of Basilica plaster layers presented in Table 1 indicated that the physical and mechanical properties of outer plaster layer (P2) is much more better than the inner plaster layer (P1). A low water absorption value and a high bulk density are beneficial for a dense, strong and durable plaster layer. Possible sources of low strength and high water absorption of inner plaster layer may be the high water/lime ratio of plaster mortar or low compactability of plaster due to high speed construction and poor workmanship. Another factor is the carbonation of lime plaster that promotes the surface hardness and hence compressive strength of outer plaster layer. It is valid that there is an incompatibility between the previously applied weak inner plaster layer and outer strong plaster layer. It was observed that some parts of these plaster layers were fully delaminate due to this incompatibility. Another possible source of high strength and hardness outer plaster layer may be the excessive trowelling of this layer for the purpose of obtaining a smooth surface suitable for graffito applications. A better compacted thin plaster layer will give higher strength and hardness values and will absorb less water compared to uncompacted one. The particle size distribution of plaster layers determined from sieve analysis revealed that maximum aggregate size of plaster layers is about 4mm and approximately 90% of the aggregates were finer than 2 mm (Figure 11). These values are in accordance with the aggregate gradation of present fine plaster formulations.

On the other hand, the load bearing capacity of Boulaterion Wall Mortars (BWM) is found much higher than that of Boulaterion Blockade Mortars (BBM) (Table 1). While, the normalized compressive strength and surface hardness values of BWM are 4.54 MPa and 37, BBM exhibited poor compressive strength (0.16 MPa) and no surface hardness value. The water absorption values were also distinctly lower for BWM compared the BBM. The low capillary porosity of BWM indicated that the water/lime ratio of these mortars are significantly lower than other mortar and plaster formulations investigated in this study. The particle size distribution graphs of BWM and BBM presented in Figure 11 revealed that aggregates of BWM is coarser than BBM and maximum aggregate size is higher than other plaster layers which are beneficial for a load bearing mortar.

3.2 Microstructural characteristics

3.2.1. Petrographic analysis results

3.2.1.1. Plaster Layers (P1,P2)

The inner (P1) and outer (P2) plaster layers are examined together in the micro-photos of Fig 12a, b. P1 is relatively thicker than the P2 as reported in Section 2.1. However, it is possible to visualize both of them at the same thin section at bonded condition (Figure 12a, b). There was a distinctive border between the plaster layers. P1 and P2 layers are mostly made up of similar matrix concentration; rock fragments and minerals. However, P1 is mostly heterogeneous and consists of anhedral calcite ($CaCO_3$) mineral pieces with typical lamellar twinning and high-birefringence colors. The sample displays rare amount of quartz (SiO_2), biotite $K(Mg,Fe^{2+})_3(Al,Fe^{3+})\ [Al,Si)_3O_{10}](OH,F)_2$ and feldspar minerals ($KAlSi_3O_8$ – $NaAlSi_3O_8$ – $CaAl_2Si_2O_8$) and total mineral abundance is not higher than 5-7% of the whole matrix.

P2 (outer layer) is composed of several sizes of calcite crystal pieces. In the P2 layer, calcites are clearly defined by their typical lamellar twinning with high-birefringence colors. Especially in the compact border to the P1 layer, the abundance of calcite crystals is more dominant that results clear and visible boundary between P2 and P1 (Figure

12a, b). Micrite-size carbonate matrix with small quartz crystals in the P2 layer give rise to become more stable relative to the P1. Long term carbon dioxide attack from the air converts the lime plaster into calcium carbonate. Carbonation results in a decrease of the porosity making the carbonated paste stronger. From this point of view the carbonation rate of P2 layer is expected to be higher than P1 since it is directly exposed to weather conditions. Since carbonated matrix appears orange-brown in crossed polarized light, both matrices of P1 and P2 layers seem affected by carbonation (Figure 12a).

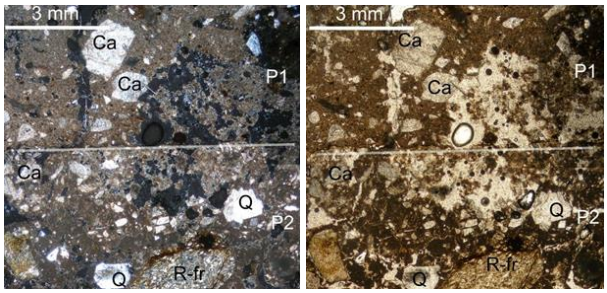

(a) *(b)*

Figure 12. Micro-photographs of the plaster layers from the Basilica Plaster Layers (P1-Inner; P2-Outer layers): a) Cross-Polarized Light (XPL) and b) Parallel Polarized Light (PPL) (Ca: Calcite, Q: Quartz, R-fr: Rock fragment, dashed line indicates the border between P1 and P2 layers, Magnification x 2.5)

3.2.1.2. Bouleuterion floor blockade mortar (BBM)

Thin sections from the BBM comprise distinct micro features compared to the P1-P2, BWM thin-sections. BBM displays homogeneous texture with various sizes of rock fragments such as sandstone, metasandstone, quartz schist, quartzite, and less amount of brick fragments (Figure 13a, b). Most of these rock fragments are semi-rounded and dominantly observed in the matrix (Figure 13a).

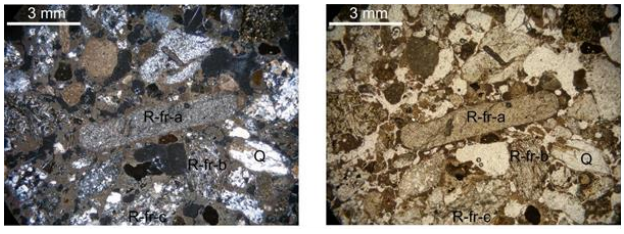

(a) *(b)*

Fig 13. Photomicrographs of the floor blockade mortar (BBM). a) Cross-Polarized Light (XPL) and b) Parallel Polarized Light (PPL) (Q: Quartz, R-fr-a: sandstone rock fragment R-fr-b: quartz-schist rock fragment, R-fr-c: metasandstone rock fragment, Magnification x 2.5)

Matrix is made up of fine grained carbonate (15-20%) and likely unconsolidated with the rock-fragments that gives rise to weak feature of the mortar. Even though, the dominant fragment character is mostly quartz (SiO_2) (75-80%), the mortar displays weak bonded features, likely porous structure, between the fragments (Figure 13a, b).

3.2.1.3. Bouleuterion wall mortar (BWM)

Micro-photos from the BWM display dominant "man-made brick" fragments spread along the mortar of the sample (Figure 14a, b). The borders of the bricks have sharp edges and they are mostly made up of micro-multi-grain minerals. These minerals are mainly subhedral quartz crystals with semi-rounded edges (Figure 14a, b). The heterogeneous abundance of these hard quartz (SiO_2) minerals may improve the overall strength of BWM mortar (Figure 14b). Abundant oxidized color is likely related to Fe-bearing µ-grains along the mortar and in the brick fragments. In addition to that, reddish mosaic piece is also observed along the thin section (Figure 14a, b). Overheated brick or a baked clay-ceramic piece, can easily display characteristic over-oxidation features.

The matrix of the BWM consists of carbonate based feature, which is whitish to yellowish in color along the thin section (Figure 14a, b). The homogeneity of this carbonate based matrix likely points out mortar's unique strength features. Biotite $K(Mg,Fe^{2+})_3(Al,Fe^{3+})[Al,Si)_3O_{10}](OH,F)_2$, pyroxene ($ABSi_2O_6$), K-feldspar ($KAlSi_3O_8$) minerals are also seen individually in the thin section. Overall, the main petrographic observations are: 48-50% brick fragment, 38-40% carbonate matrix, 4-6% quartz, and 2-4% other minerals as described above.

3.2.1.4. SEM-EDS analysis results

Secondary electron (SE) images of P1 and P2 plaster layers with the boundary region captured at 30x magnification is presented in Fig 15a. While the P2 plaster layer (outer) is comparatively more compact, P1 plaster layer (inner) exhibit more porosity. In some sections polishing was not possible due to the weak matrix structure of P1 plaster layer. A linear EDS analysis has been performed from the point A to B in order to observe the element distribution (Ca, Si, Al, Fe, O, Na, K, Mg) of P1 and P2 plaster layers (Figure 15a red line) (Riccardi et al., 2007). Both plaster layers are mainly composed of Ca element and Si, Al, Na and K elements were observed when the aggregates exposed to the polished surface (Figure 15b). Other elements detected as traces (Figure 15c). These results are in conformity with the chemical compositions of the detected aggregate types (quartz, biotite and feldspar minerals) from petrographic analysis.

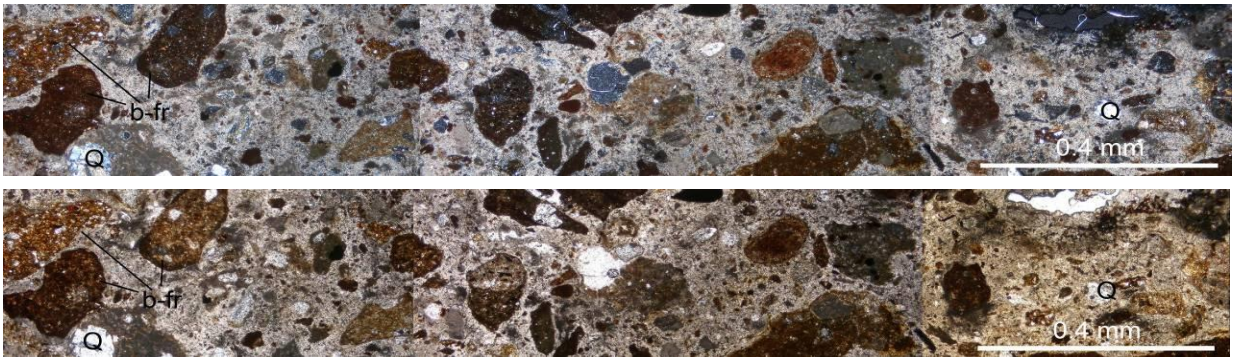

Figure 14. Combined photomicrographs of the Bouleuterion wall mortar (BWM). a) Cross-Polarized Light (XPL) and b) Parallel Polarized Light (PPL) (Q: Quartz, b-fr: brick fragments, Magnification x 2.5)

A rectangular area plotted in Figure 15a is also analyzed to determine the composition of matrix phase of P1 plaster. EDS analysis indicated the existence of C (23.2%), O (24.8%) and Ca (51%) elements respectively. This composition is significantly different from the theoretical composition of calcite (C(12%), Ca(40%), and O(48%)). Note that unexpected high amount of C atom may arise from the carbon band background which was used to provide the conductivity of specimen. A small amount of Si element (1.1%) is also detected possibly due to the presence of aggregates close to the surface of polished section. A closed view of a point captured at 2000x magnification from this rectangular area is presented in Figure 16. Based on crystal morphology observed in this figure, these formations may be micritic calcite ($CaCO_3$) crystals which previously formed due to the carbonation of lime (Çizer et al., 2008).

Some traces of natural fibers were also detected in P1 plaster (Figure 15a, marked with red circle). These traces were possibly due to the addition of short cut wood fibers into the P1 plaster mortar at fresh state. Fiber addition may improve the cracking resistance of plaster mortars by bridging the cracks. Another advantage of addition of natural fibers is the decrease in the unit weight of plaster which brings application easiness. However, natural cellulose based fibers may degrade in alkaline environments. Since lime-based mortars are highly alkaline these fibers may deteriorate with time and possibly only their traces are observable. It should be noted that a lightweight plaster incorporating high amounts of pores (previously fibers) also exhibit mechanical weakness.

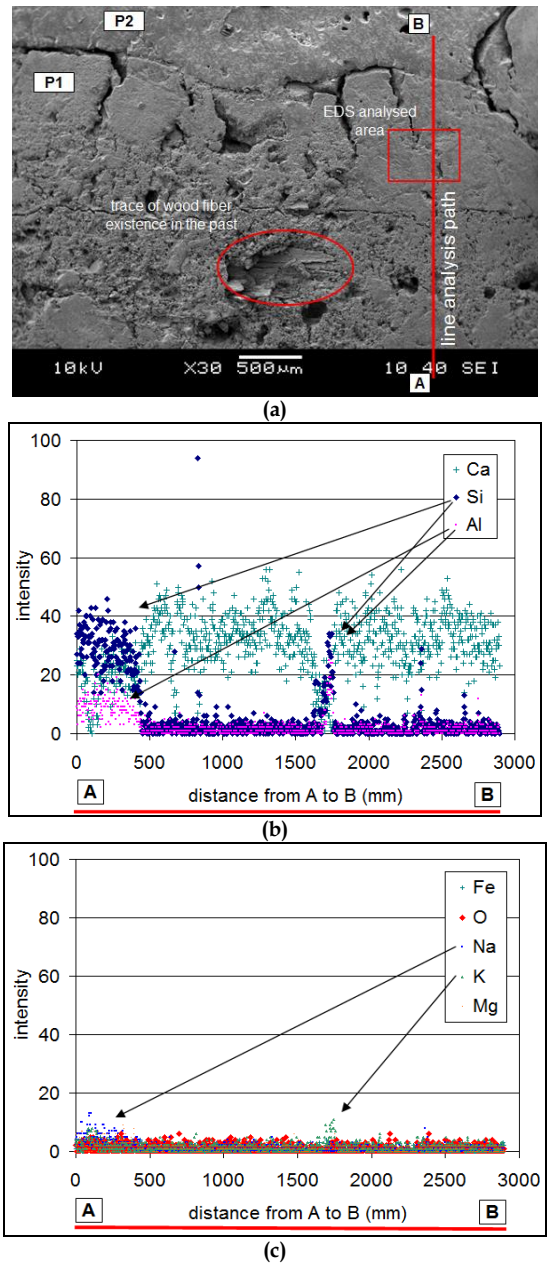

Figure 15. SE images of P1 and P2 plaster layers with the boundary region captured at 30x magnification (a), line analysis results Ca, Si, Al (b), line analysis results Fe, O, Na, K, Mg.

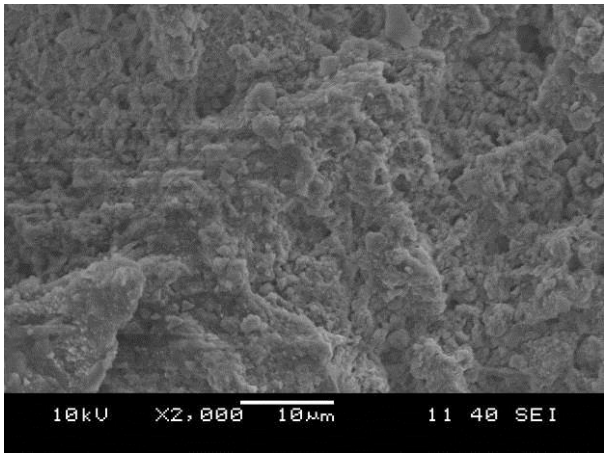

Figure 16. Micritic calcite ($CaCO_3$) crystals which previously formed due to the carbonation of lime

SEM observations of BWM specimens indicated a high brick fragment-matrix cohesion which formed due to the previous formation of pozzolanic reaction between the amorphous silicate based components of brick fragments and lime (Moropoulou et al., 2002). The resultant calcium silicate hydrates may be responsible for the high compressive strength and low water absorption values of BWM. On the other hand BBM is more porous and there is no evidence of brick fragment presence which may limit the formation of any calcium silicate hydrates at the aggregate-matrix interface. The resultant mechanical properties were limited and high water absorption values were recorded for BBM specimens.

3.2.2. XRD analysis results

XRD patterns of powders finer than 63 μm of all plaster and mortar specimens are presented in Figure 17a. Since the calcite peaks are distinct at all XRD patterns, the binder phase of all specimens are initially composed of lime and time dependent carbonation reactions converted all lime into calcite (Böke et al., 2004). No trace of Portlandite crystal peaks was found in any of specimens which indicated that all lime is converted to calcite. Quartz peaks were also visible in the case of Boulaterion specimens. This might be due to the grinding of aggregates composed of quartz based minerals. Quartz and feldspar peaks were observed at XRD patterns of coarser powders of plaster specimens (63-125 μm), which may be mixed to binder phase from crushed aggregates (Figure 17b) (Riccardi et al., 1998; Böke et al., 2006). The source of lime (slaked or hydraulic) is not clarified from XRD peaks since low amounts of amorphous phases can not be detected from XRD difraktogram.

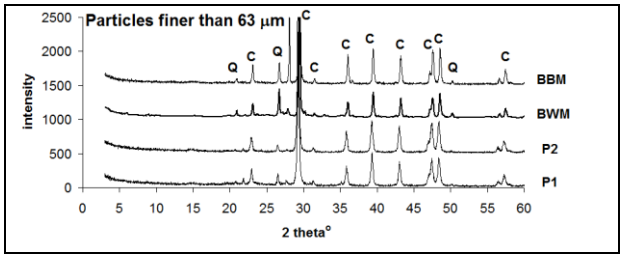

(a)

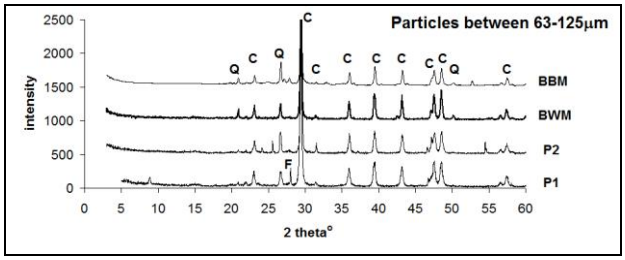

(b)

Figure 17. XRD patterns of; a) powders finer than 63 μm, b) powders between 63-125 μm (C=Calcite, Q=Quartz, F=Feldspar)

4. CONCLUSIONS

Physical and mechanical characterization studies performed on Basilika graffito plaster layers indicated that the plaster layers exhibit distinctly different properties in terms of bulk density, water absorption, hardness and strength. While the outer plaster layer was dense, relatively less permeable, hard and strong in compression, the inner plaster layer was weak and exhibited a porous permeable structure. Micro-analysis results showed that both plaster layers were fully carbonated (calcite crystals detected by XRD and SEM analysis). The strength and bulk density differences between plaster layers can be attributed to the initial mixing water content and compaction efficiency of plasters at the stage of plaster preparation and application. Presence of high amounts of mixing water increases the capillary porosity of inner plaster layer. Poor workmanship at the stage of application of inner plaster layer may also contribute to the low strength of this plaster. On the other hand, relatively low water content reduced the capillary porosity and forced troweling attempts improved the compactability of outer layer plaster at the same time. Another factor that reduces the density of inner plaster layer is the presence of wood fiber traces (detected by SEM observations) throughout the matrix which deteriorated with time and caused a porosity increase.

Experimental studies on Boulaterion mortar specimens indicated that BWM is relatively denser, stronger and absorb less water compared to BBM specimens. Petrographic investigations on thin sections of BWM showed that this mortar contains con-

siderable amounts of man made brick fragments and powder. The slow pozzolanic reaction between the amorphous silicate portion of these brick fragments and lime and or hydraulic lime present in mortar composition contributes to the formation of calcium silicate hydrate based products. These load bearing phases may possibly improve the strength and impermeability of matrix and aggregate interface. Furthermore a compact and homogeneous matrix structure is observed in the case of BWM. However, BBM is weak in compression and relatively more water permeable in the absence of brick fragment addition which indicates that only the carbonation is responsible for strength and permeability of mortar. Another source of high capillary porosity of BBM might be the relatively high mixing water content of this mortar. Since this mortar should fill the spaces between blockade stones, a low viscosity is preferential for application easiness. Furthermore no compaction is necessary at the application of this mortar. Due to these reasons, the extra mixing water employed in BBM may reduce its mechanical properties and water transport resistance respectively.

REFERENCES

Alejandre, F. J., Flores-Ales, V., Villegas, R., Garcia-Heras, J., & Moron, E. (2014). Estimation of Portland cement mortar compressive strength using microcores. Influence of shape and size. *Construction and Building Materials*, Vol. 55, 359-364.

Böke, H., Akkurt, S., & İpekoğlu, B. (2004). Tarihi yapılarda kullanılan Horasan harcı ve sıvalarının özellikleri. *Yapı Dergisi*, Vol. 269, 90-95.

Böke, H., Akkurt, S., İpekoğlu, B., & Uğurlu, E. (2006). Characteristics of brick used as aggregate in historic brick-lime mortars and plasters. *Cement and Concrete Research*, Vol. 36(6), 1115-1122.

Cizer, Ö., Van Balen, K., Elsen, J., & Van Gemert, D. (2008). Crystal morphology of the precipitated calcite crystals from accelerated carbonation of lime binders. *In 2nd International Conference on Accelerated Carbonation for Environmental and Materials Engineering,* 149-158.

de Vekey, R. C. (1997). A review of the work of the RILEM committee 127-MS: testing masonry materials and structures. *Materials and Structures*, Vol. 30(1), 12-16.

Franzini, M., Leoni, L., & Lezzerini, M. (2000). A procedure for determining the chemical composition of binder and aggregate in ancient mortars: its application to mortars from some medieval buildings in Pisa. *Journal of Cultural Heritage*, Vol. 1(4), 365-373.

Moropoulou, A., Bakolas, A., & Bisbikou, K. (2000). Physico-chemical adhesion and cohesion bonds in joint mortars imparting durability to the historic structures. *Construction and Building Materials*, Vol. 14(1), 35-46.

Moropoulou, A., Cakmak, A. S., Biscontin, G., Bakolas, A., & Zendri, E. (2002). Advanced Byzantine cement based composites resisting earthquake stresses: the crushed brick/lime mortars of Justinian's Hagia Sophia.*Construction and Building Materials*, Vol. 16(8), 543-552.

Proceq Schmidt OS-120 (2014). *Pendulum Hammer Operating Instructions Manual*, 14p.

Riccardi, M. P., Duminuco, P., Tomasi, C., & Ferloni, P. (1998). Thermal, microscopic and X-ray diffraction studies on some ancient mortars.*Thermochimica Acta*, Vol. 321(1), 207-214.

Riccardi, M. P., Lezzerini, M., Carò, F., Franzini, M., & Messiga, B. (2007). Microtextural and microchemical studies of hydraulic ancient mortars: two analytical approaches to understand pre-industrial technology processes. *Journal of Cultural Heritage,* Vol. 8(4), 350-360.

Schueremans, L., Cizer, Ö., Janssens, E., Serré, G., & Van Balen, K. (2011). Characterization of repair mortars for the assessment of their compatibility in restoration projects: research and practice. *Construction and Building Materials*, Vol. 25(12), 4338-4350.

TS EN 196-1 (2009). *Methods of testing cement - Part 1: Determination of strength*, 31p.